Photoconducting response on bending of individual ZnO nanowires†‡

P. Gao, Z. Z. Wang, K. H. Liu, Z. Xu, W. L. Wang, X. D. Bai* and E. G. Wang*

The bending effect of individual zinc oxide (ZnO) nanowires on photoconducting behavior has been investigated by an *in situ* transmission electron microscopy (TEM) method. By increasing the nanowire bending, the photocurrent of ZnO nanowire under ultraviolet illumination drops dramatically and the photoresponse time becomes much shorter. A possible mechanism has been proposed and discussed. The improved photo response performance by bending ZnO nanowires could be of significance for their optoelectronics and sensor applications.

Introduction

Due to their unique electronic, optical, and piezoelectric properties, zinc oxide (ZnO) semiconducting nanowires are considered as an important multifunctional building block for fabricating various nanodevices, such as field effect transistors,[1–5] optically pumped lasers,[6–8] photodetectors, optical switches,[9–17] and sensors.[18–23] Recently, the nanogenerators,[24] piezoelectric field effect transistors,[25] and piezoelectric diodes[26] based on ZnO nanowires have been developed by the coupling of piezoelectric and semiconducting properties of ZnO. Despite the abundant research on semiconduting, piezoelectric and optoelectronic properties of the ZnO nanowires, the coupling between the optoelectronic property and the piezoelectric property is rarely reported, which is of significance for their applications in optoelectronics and sensor technologies and also could light on the fundamental research of this material, such as the internal electronic structure, the surface effect and the piezoelectric-dependent optoelectric transport. In this paper, we present a systematic study of the photoconducting response on the bending of individual ZnO nanowires by an *in situ* transmission electron microscopy (TEM) method.

Experimental

The ZnO nanowires used in our experiments were synthesized by the thermal evaporation of ZnO powders.[27] The details are given in the supplementary information.‡ In order to probe the fundamental physical properties of a single nanowire, an *in situ* TEM measurement system was built inside a JEOL 2010 FEG TEM, operated in 10^{-5} Pa vacuum and at room temperature, which has been used to study the mechanical properties of nanowires,[28] field emission properties of carbon nanotubes,[29] and electrical transport of ZnO nanowires.[30] Our experimental setup is schematically shown in Fig. 1(a). An LED chip, beside the ZnO nanowire, was fixed on the frame of the specimen holder. The

peak of the LED's emission spectrum is at $\sim$380 nm,[31–33] and its full-width-at-half-maximum (FWHM) is $\sim$10 nm. To carry out photoelectrical measurements inside TEM, the ZnO nanowire was attached to the Pt tip with silver paint, then heated at 393 K for 20 min to form a good electric contact.[25] The Pt tip with ZnO nanowire was then loaded to the specimen holder, and was approached to its opposite electrode (Pt) by a piezo-manipulator. In order to achieve an improved electrical contact between the ZnO nanowire and the Pt tip, the following two steps were adopted. At the first step, a field emission process was introduced to clean the nanowire's top end. The distance between the nanowire and its opposite electrode is several micrometres, and a relatively high voltage $\sim$400 V is applied. The field emission current could reach as high as hundreds of nano-amperes. After 1 min of emission, the high voltage was turned off, and the Pt tip was moved toward the ZnO nanowire to contact and bend it a little. At the second step, we applied a voltage $\sim$50 V between the two electrodes with transport current from tens to hundreds of nano-amperes, for 1 min again. Because of the high resistance at the contact points of nanowire ends, a local high temperature generated by the Joule heating could weld the nanowire onto its electrode, such that a stable electrical contact is realized.[25,34] While performing the electrical measurements, the TEM electron beam was blacked out to rule out the influence of electron bombardment.

Results and discussion

Fig. 1(b) shows a ZnO nanowire clamped between two Pt electrodes. Fig. 1(c) shows the corresponding *I–V* characteristics curves (using Keithley 2400 and 6487) of the ZnO nanowire in dark and under UV illumination, obtained by sweeping the voltage from −5 to 5 V. The current through the nanowire increases obviously under UV illumination. Because the electron-hole pairs are photogenerated under illumination with photon energy larger than the band gap (E_g), and the holes are readily trapped at the surface, leaving behind unpaired electrons, which increases the conductivity under an applied electric field.[9,10,13,17,20,35] There is an important point to be noted, that is the symmetrical shape of the ZnO nanowire.

The ZnO nanowire was examined at a high TEM magnification before the formation of the contact, as shown in Fig. 2(a).

Beijing National Laboratory for Condensed Matter Physics and Institute of Physics, Chinese Academy of Sciences, Beijing, 100190, China. E-mail: xdbai@aphy.iphy.ac.cn; egwang@aphy.iphy.ac.cn
† This paper is part of a *Journal of Materials Chemistry* theme issue on Nanotubes and Nanowires. Guest editor: Z. L. Wang.
‡ Electronic supplementary information (ESI) available: Synthesis and characterization of the ZnO nanowires. See DOI: 10.1039/b816791e
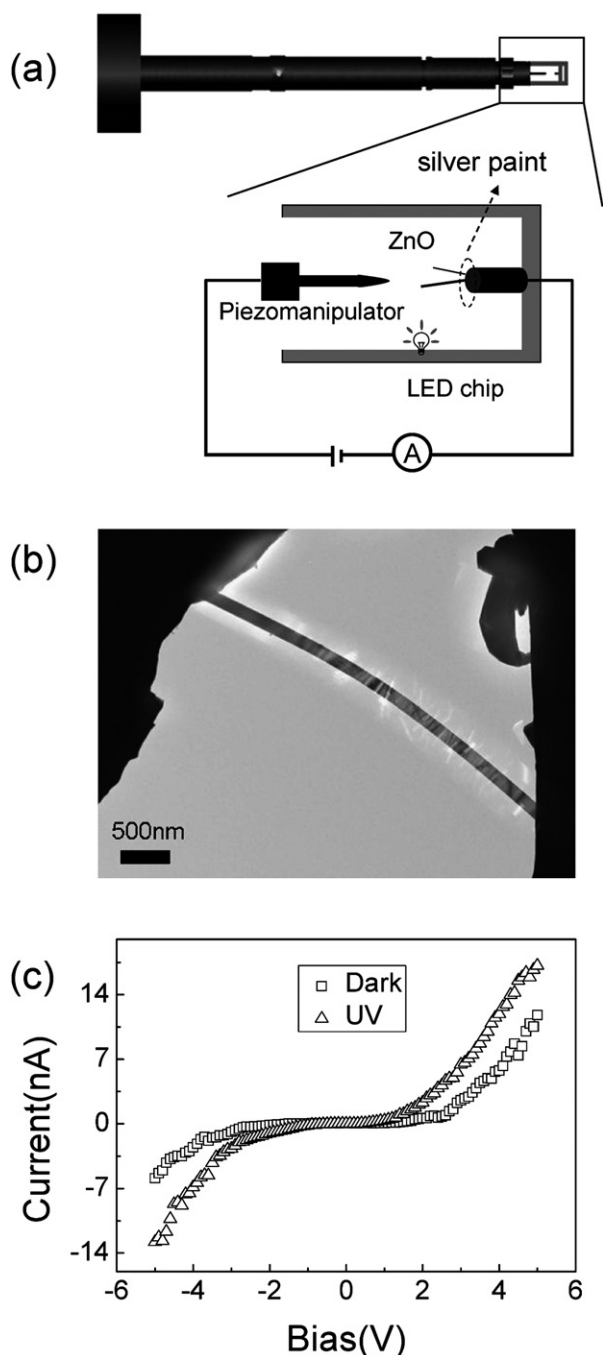
Fig. 1 (a) A setup for *in situ* TEM photoelectric measurements. ZnO nanowires are attached on Pt wires (right electrode) with silver paint. Another Pt probe (left electrode) is driven to approach the ZnO nanowire by a three-dimensional piezo-manipulator. An LED chip is fixed on the frame of the specimen holder. (b) A ZnO nanowire is clamped between two Pt electrodes. (c) Corresponding *I–V* characteristics curves of the ZnO nanowires in dark (squares) and under illumination (triangles), respectively.

The length of the nanowire is ∼3.2 μm, and its diameter is ∼198 nm. The SAED pattern (inset of Fig. 2(a)) indicates a single-crystalline structure of the ZnO nanowire and its growth direction is along [0001]. With the same magnification, Fig. 3(b)–3(d) show the three typical bending cases during a sequential bending
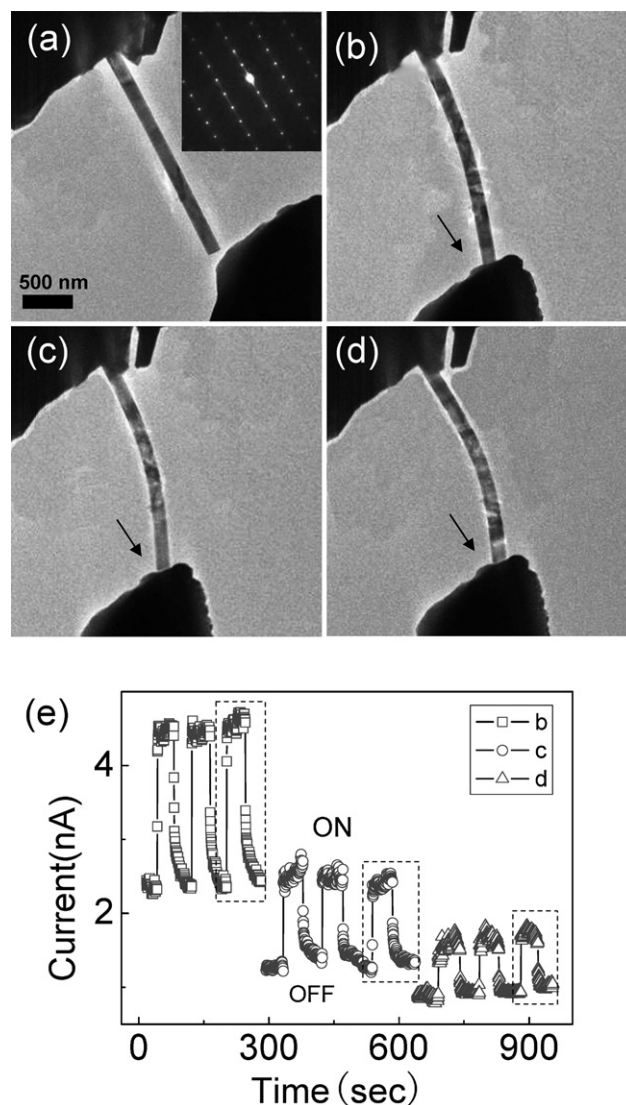
Fig. 2 (a) TEM image showing a stationary ZnO nanowire before contacting, and the inset is its electron diffraction pattern. (b)–(d) The three typical bending cases of the ZnO nanowire from a sequential bending process. The arrows show no sliding during the bending process. (e) Corresponding *I–V* characteristics of the ZnO nanowire for the three different bending cases. Both of the dark current and photocurrent decrease with the increase of bending. Squares: (b); circles: (c); triangles: (d).

process of the ZnO nanowire by gently moving the piezo-driven Pt tip. No sliding at the contact point between the nanowire and its electrode was observed, as shown by the arrowheads inset.

The electrical transport properties of bent ZnO nanowire with increasing bending were recorded under dark and UV illumination conditions, as shown in Fig. 2(e). At a bias of 5 V, the currents increased upon illumination, and then decayed to a stable value after the light was turned off. The currents both in dark and under illumination decreases when the nanowire is bent, indicating the conductance reduced with increasing strain. Fig. 3 is the enlarged view of the rectangle regions in Fig. 2(e), which shows the decay curve consists of two slopes: the fast decay first and then a slow decay tail; the slow decay tail became shorter with the increase of bending. These phenomena could be
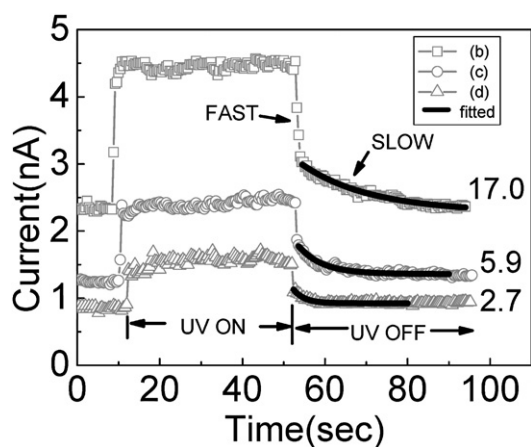
Fig. 3 The enlarged view of the rectangle region in Fig. 2(e), the decay time becomes shorter with the increase of bending. Squares: Fig. 2(b); circles: Fig. 2(c); triangles: Fig. 2(d). The decay tails are fitted by the exponential time dependency $I = I_0\exp(-t/\tau_{dt})$. The τ_{dt} are 17.0 s, 5.9 s and 2.7 s respectively, corresponding to the bending cases in Fig. 2(b), (d), and (d), respectively.

attributed to the change of internal electronic structure of the bent ZnO nanowire.

A bent ZnO nanowire can produce a positively charged and negatively charged surface at its outer and inner bending arc surfaces due to the stretching and compression on the surfaces, respectively.[24,25] The charges are static and nonmobile ionic charges, thus, a small electric field would be induced across the width of the ZnO nanowire, as schematically shown in the cross-section image of the nanowire in Fig. 4(a). The electric field is generated across the width of the ZnO nanowire while bending, the reduction of the nanowire's conductance can be accounted to
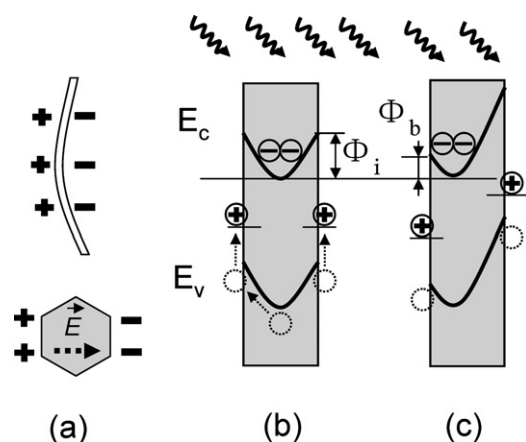
Fig. 4 Schematic diagrams of the proposed mechanism for the change of the photocurrent and the photoresponse speed. (a) The piezo-induced electric field due to the nonmobile ionic charges at the surface when the nanowire is bent. The current drops due to the carrier trapping effect and the reduction of the conducting channel. (b) The case for an unbent nanowire: the conduction and valence band edges are bent near the surface owing to the surface Fermi-level pinning. Electrons prefer in the inner part, whereas the holes tend to migrate to the surface and be trapped. Φ_i is the intrinsic surface recombination barrier. (c) The case for a bent nanowire: the piezo-induced electric field lowers the surface recombination barrier from Φ_i to Φ_b.

the following two reasons: some free electrons are trapped at the outer arc surface (positive side surface) and become nonmobile charges, so that the effective carrier density is lowered in the ZnO nanowire as a *n*-type semiconductor. On the other hand, the free electrons are repulsed away by the piezo-induced electric field across the width of the nanowire. Consequently, the width of the conducting channel in the ZnO nanowire becomes narrower with the increase of the bending. So the carrier trapping effect and the reduction of the conducting channel result in the decrease of the conductance of the ZnO nanowire with the increase of bending.

A possible model is proposed to clarify the origin of the slower decay tail with the increase of bending (Fig. 3). Because of the surface Fermi-level pinning within the forbidden band, the *n*-type ZnO nanowires exhibit a depletion space charge layer near the surface.[9,20,31,35–39] The ZnO nanowire can be depleted completely or partly, depending on the wire thickness, dopant, and atmosphere. The depletion space charge layer results in the electric bands, conduction (E_c), and valence (E_v), being bent upward at the surface of the ZnO nanowire, as shown schematically in Fig. 4(b). Thus the photo-excited electrons prefer to stay in the inner part of the column, whereas the holes tend to migrate to the surface. Owing to the high surface-to-volume ratio of the nanowire, the holes are readily trapped at the surface. It could be understood that the recombination of the carriers *via* surface traps in the forbidden band is the prevailing recombination mechanism.[37] Due to the spatial separation of the photo-excited holes and electrons, the recombination of non-equilibrium carriers is reduced. So the electrons would have to surpass the conduction band barrier Φ (Fig. 4(b)) at the surface for the recombination. Actually, the recombination rate is basically fitted by an exponential term $\exp(-\Phi/kT)$,[37] when the decay time of the persistent photocurrent is mainly resulted from the surface recombination, the holes are pushed to the surface due to band bending and electrons have to overcome the corresponding surface barrier in order to recombine. When the nanowire is bent, the energy band is modified by the piezo-induced electric field. Both the conduction band and valence band are upward near the negative charge surface side, and downward near its opposite side, as shown in Fig. 4(c). The barrier of bending case Φ_b (Fig. 4(c)) is lower than that of Φ_i (Fig. 4(b)), which is the intrinsic recombination barrier only caused by the depletion space charge layer near the surface. Because of the decrease of Φ_b, the recombination rate will increase when the nanowire is further bent. As mentioned before, the decay process consists of two parts, the fast decay and the slow decay tail. The appearance of the slow decay tail is believed to be associated with the recombination barrier.[37,38] Thus, the slow decay time becomes shorter with the increase of bending. We fitted the decay tails with the exponential dependency $I = I_0\exp(-t/\tau_{dt})$,[40] where the τ_{dt} indicates how fast the decay is. Fig. 3 shows the τ_{dt} are 17.0 s, 5.9 s and 2.7 s, respectively, corresponding to the bending cases in Fig. 3(b), (c) and (d). It is indicated that the photoresponse time greatly becomes shorter with an increase of nanowire bending, which is of significance for the optoelectronics and sensor applications of ZnO nanowires.

Conclusions

In conclusion, we have studied the electrical transport coupled with the optical and piezoelectric properties of individual ZnO

nanowires by an *in situ* TEM method, which also allows a direct investigation of the property and the structure. It is found that the photocurrent drops and the decay time largely decreases with the increase of bending of the ZnO nanowire. The reduction of the conductance is attributed to the charge trapping effect and the decrease of the conducting channel, due to the piezo-induced electric field when the ZnO nanowire is bent, and the slow decay tail of the photocurrent is resulted from the surface recombination barrier. The fitted data shows that the photoresponse speed becomes much higher when the ZnO nanowire is further bent. The possible reason is that the piezo-induced electric field lowers the surface recombination barrier, thus the surface recombination rate increases and the time of decay tail reduces. The improved photoresponse speed might shed light on the design of novel opto-piezoelectronic devices and sensors.

References

1   J. Goldberger, D. J. Sirbuly, M. Law and P. Yang, *J. Phys. Chem. B*, 2005, **109**, 9.
2   H. T. Ng, J. Han, T. Yamada, P. Nguyen, Y. P. Chen and M. Meyyappan, *Nano Lett.*, 2004, **4**, 1247.
3   Z. Y. Fan and J. G. Lu, *Appl. Phys. Lett.*, 2006, **86**, 032111.
4   P. C. Chang, Z. Fan, C. J. Chien, D. Stichtenoth, C. Ronning and J. G. Lu, *Appl. Phys. Lett.*, 2006, **89**, 133113.
5   S. H. Ju, K. Lee and D. B. Janes, *Nano Lett.*, 2005, **5**, 2281.
6   M. H. Huang, S. Mao, H. Feick, H. Q. Yan, Y. Y. Wu, H. Kind, E. Weber, R. Russo and P. D. Yang, *Science*, 2001, **292**, 1897.
7   B. S. Zou, R. Liu, F. Wang, A. Pan, L. Cao and Z. L. Wang, *J. Phys. Chem. B*, 2006, **110**, 12865.
8   P. J. Pauzaukie and P. Yang, *Mater. Today*, 2006, **9**, 36.
9   H. Kind, H. Yan, B. Messer, M. Law and P. Yang, *Adv. Mater.*, 2002, **14**, 158.
10 J. B. K. Law and J. T. L. Thong, *Appl. Phys. Lett.*, 2006, **88**, 133114.
11 L. Luo, Y. F. Zhang, S. S. Mao and L. W. Lin, *Sens. Actuators, A*, 2006, **127**, 201.
12 R. Konenkamp, R. C. Word and C. Schlegel, *Appl. Phys. Lett.*, 2004, **85**, 6004.
13 S. Kumar, V. Gupta and K. Sreenivas, *Nanotechnology*, 2005, **16**, 1167.
14 Y. W. Heo, L. C. Tien, D. P. Norton, B. S. Kang, F. Ren, B. P. Gila and S. J. Pearton, *Appl. Phys. Lett.*, 2004, **85**, 2002.
15 C. L. Hsu, S. J. Chang, Y. R. Lin, P. C. Li, T. S. Lin, S. Y. Tsai, T. H. Lu and I. C. Chen, *Chem. Phys. Lett.*, 2005, **416**, 75.
16 K. Keem, H. Kim, G. T. Kim, J. S. Lee, B. Min, K. Cho, M. Y. Sung and S. Kim, *Appl. Phys. Lett.*, 2004, **84**, 4376.
17 Z. Y. Fan, P. C. Chang, J. G. Lu, E. C. Walter, R. M. Penner, C. H. Lin and H. P. Lee, *Appl. Phys. Lett.*, 2004, **85**, 6128.
18 Q. Wan, Q. H. Li, Y. J. Wang, T. H. Wang, X. L. He, J. P. Li and C. L. Lin, *Appl. Phys. Lett.*, 2004, **84**, 3654.
19 Z. Y. Fan, D. W. Wang, P. C. Chang, W. Y. Tseng and J. G. Lu, *Appl. Phys. Lett.*, 2004, **85**, 5923.
20 Q. H. Li, Y. X. Liang, Q. Wan and T. H. Wang, *Appl. Phys. Lett.*, 2004, **85**, 6389.
21 Z. Y. Fan and J. G. Lu, *IEEE Trans. Nanotechnol.*, 2006, **5**, 393.
22 T. J. Hsueh, S. J. Chang, C. L. Hsu, Y. R. Lin and I. C. Chen, *Appl. Phys. Lett.*, 2007, **91**, 05311.
23 Z. L. Wang, *Annu. Rev. Phys. Chem.*, 2004, **55**, 159.
24 Z. L. Wang and J. H. Song, *Science*, 2006, **312**, 242.
25 X. D. Wang, J. Zhou, J. H. Song, J. Liu, N. S. Xu and Z. L. Wang, *Nano Lett.*, 2006, **6**, 2768.
26 J. H. He, C. L. Hsin, J. Liu, L. J. Chen and Z. L. Wang, *Adv. Mater.*, 2007, **19**, 781.
27 Z. W. Pan, Z. R. Dai and Z. L. Wang, *Science*, 2001, **291**, 1974.
28 K. H. Liu, W. L. Wang, Z. Xu, L. Liao, X. D. Bai and E. G. Wang, *Appl. Phys. Lett.*, 2006, **89**, 221908.
29 Z. Xu, X. D. Bai, E. G. Wang and Z. L. Wang, *Appl. Phys. Lett.*, 2005, **87**, 163106.
30 K. H. Liu, P. Gao, Z. Xu, X. D. Bai and E. G. Wang, *Appl. Phys. Lett.*, 2008, **92**, 213105.
31 C. Soci, A. Zhang, B. Xiang, S. A. Dayeh, D. P. R. Aplin, J. Park, X. Y. Bao, Y. H. Lo and D. Wang, *Nano Lett.*, 2007, **7**, 1003.
32 I. Shalish, H. Temkin and V. Narayanamurti, *Phys. Rev. Lett. B*, 2004, **69**, 245401.
33 Z. L. Wang, *J. Phys.: Condens. Matter*, 2004, **16**, R829.
34 S. M. Sze, *Physics of Semiconductor Devices*, John Wiley & Sons, Inc, New York, 1981.
35 Q. H. Li, Q. Wan, Y. X. Liang and T. H. Wang, *Appl. Phys. Lett.*, 2004, **84**, 4556.
36 H. Luth, *Solid Surfaces, Interfaces and Thin Films*, 4th edn, Springer, Berlin, Heidelberg, 2001, (ch. 7).
37 R. Calarco, M. Marso, T. Richter, A. Aykanat, R. Meijers, A. v. d. Hart, T. Stoica and H. Luth, *Nano Lett.*, 2005, **5**, 981.
38 J. S. Liu, W. J. Zhang, Y. Jiang, X. M. Meng, Y. Q. Li and S. T. Lee, *Nano Lett.*, 2006, **6**, 1887.
39 Z. M. Liao, K. J. Liu, J. M. Zhang, J. Xu and D. P. Yu, *Phys. Lett. A*, 2007, **367**, 207.
40 N. V. Joshi, *Photoconducivity: Art, Science, and Technology*, Marcel Dekker, Inc., New York, 1990.

This journal is © The Royal Society of Chemistry 2009

J. Mater. Chem., 2009, **19**, 1002–1005 | 1005